ACS OMEGA

http://pubs.acs.org/journal/acsodf

Article

Nonlinear Absorption and Refraction of Highly Monodisperse and Luminescent ZnTe Quantum Dots and Their Self-Assembled Nanostructures: Implications for Optoelectronic Devices

Sovan Kumar Patra,[#] Bhavesh Kumar Dadhich,[#] Bhavya Bhushan, Ravi Kant Choubey, and Amiya Priyam*

Cite This: *ACS Omega* 2021, 6, 31375−31383

Read Online

ACCESS | Metrics & More | Article Recommendations | Supporting Information

ABSTRACT: Zinc telluride (ZnTe) quantum dots (QDs) were synthesized by a unique supersaturation-controlled aqueous route. For a given pH, increasing the degree of initial supersaturation led to a decrease in the average diameter (d_{avg}) of the QDs and increased monodispersity. Three samples of ZnTe QDs having average sizes of 0.8, 1.7, and 2.2 nm were synthesized (hence named ZnTe_0.8, ZnTe_1.7, and ZnTe_2.2). Nonlinear absorption (NLA) and nonlinear refraction (NLR) of these colloidal ZnTe QDs of different sizes were investigated by the *Z*-scan technique using a continuous He−Ne laser (632.8 nm, 15 mW). Isotropic assembly of ZnTe_2.2 leads to the formation of nanoballs (hence named ZnTe_NB). The NLA profile of smaller QDs, ZnTe_1.7 and ZnTe_0.8, was found to follow a three-photon absorption (3PA) model, while relatively bigger QDs, ZnTe_2.2, followed a two-photon absorption (2PA) model. On moving from ZnTe_0.8 to ZnTe_1.7, the three-photon absorption coefficient (γ) decreases by 26% ($3.00 \times 10^{-4} \rightarrow 2.21 \times 10^{-4}$ cm^3/MW^2). The two-photon absorption coefficient (β) for ZnTe_2.2 is 0.3 cm/MW. For a 63% decrease in average diameter (2.2 → 0.8 nm), the refractive index (n_2) increases by 45% ($2.48 \times 10^{-2} \rightarrow 3.6 \times 10^{-2}$ cm^2/MW). Overall, the NLR coefficient shows a decreasing trend with size. Upon isotropic self-assembly, ZnTe_NB, there is a significant increase in the NLR coefficient by 40% ($2.48 \times 10^{-2} \rightarrow 3.48 \times 10^{-2}$ cm^2/MW) and a simultaneous decrease in the NLA coefficient by 45% (0.3 → 0.166 cm/MW). The figure of merit was also determined for all of the samples, and it was found that ZnTe_2.2 and ZnTe_0.8 were best suited for all-optical device applications. Further, the self-assembled nanostructures are promising for making optical waveguides for supercontinuum generation (SCG).

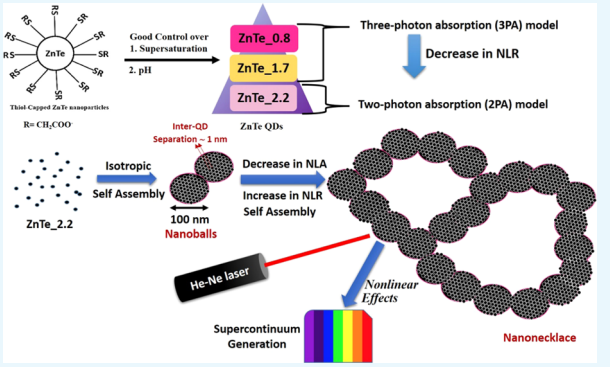

1. INTRODUCTION

Colloidal semiconductor nanocrystals or quantum dots (QDs) have been extensively studied for their size-tunable absorption and luminescence properties, which has further found scientific progress into diverse applications such as bioimaging, biosensing, catalysis, lighting, and photovoltaics.[1,2] The genesis of the unusual optical properties lies in the spatial confinement of charge carriers, electrons, and holes in these nanocrystals.[3,4] Due to the quantum confinement phenomenon, QDs are also expected to be a strong candidate in the field of nonlinear optics. They have been found to possess large and fast nonlinear optical (NLO) response and excellent thermochemical stability, making them suitable for data storage and optical telecommunication applications.[5,6] In addition to device-making, recent efforts in integrating the NLO signals with scanning microscopy have provided new perspectives in bioimaging.[7−9] The novel NLO microscopy has some inherent advantages as it can give 3D spatial resolution, which conventional scanning microscopy cannot provide. Furthermore, it has greater tissue penetration as near-infrared (NIR) lasers are employed, which also helps minimize the unwanted photodamage to the healthy cells.[10]

The development of NLO-based biomedical techniques and devices is an interesting yet challenging task. For such applications, there is a need to comprehend the NLO properties of nanomaterials. Although many QD-based NLO materials have been explored for optical limiting (OL) and switching applications,[11−13] there is still an adequate scope to fine-tune the optical nonlinearities of the QDs. Semiconductor QDs, such as CdS,[14,15] CdSe,[16] CdTe,[17,18] ZnS,[19,20] ZnO,[21,22] etc., have been extensively investigated, however, there is hardly any report on NLO properties of ZnTe QDs.

Received: September 30, 2021
Accepted: October 26, 2021
Published: November 9, 2021

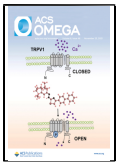

Scheme 1. Experimental Setup for the Closed-Aperture Z-Scan Technique[a]

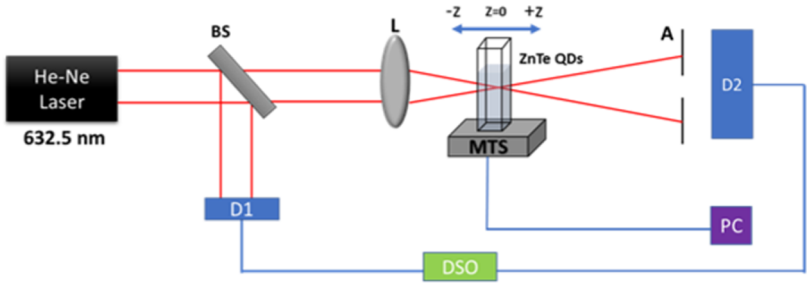

[a]BS: beam splitter; L: focusing lens; A: aperture; D1 and D2: detectors; MTC: motorized translation stage; DSO: digital storage oscilloscope; PC: computer; and Z is the distance from the focus.

Fundamentally, ZnTe QDs belong to the class of II−VI semiconductor nanocrystals and have a direct band gap of 2.26 eV.[23] It is quite suitable for photocatalytic and photovoltaic applications due to a highly negative (−1.7 V vs NHE) conduction band-edge position.[24] ZnTe QDs are also promising for biomedical applications as the toxicity of zinc is much less as compared to cadmium.

In addition to robust linear optical properties, ZnTe QDs are also expected to have large third-order optical nonlinearity ($\chi^{(3)}$).[25] Du et al.[26] reported NLO properties of ZnTe QDs trapped in ZnO−TeO_2−P_2O_5 (ZTP) glasses, however, there was no control over particle sizes and the optical absorption spectra were too broad. We previously reported a unique supersaturation-controlled method to synthesize highly monodisperse, water-soluble ZnTe QDs with enhanced tunability of size and luminescence.[23] The initial degree of supersaturation provides a tool to control the subsequent processes of nucleation and growth, which, in turn, affects the particle size, size distribution, and crystallinity of the QDs. Their effect on NLO properties is a key aspect, which has been rather unexplored till now. It is also not known how the self-assembly of colloidal QDs[23,27] could alter the nonlinear absorption and refraction.

In the present work, nonlinear absorption (NLA) and nonlinear refraction (NLR) of differently sized colloidal ZnTe QDs have been investigated by the open- and closed-aperture Z-scan technique at 632.8 nm using a continuous-wave (CW) laser at a low power of 15 mW. The QD sizes range from subnanometer to 2.2 nm, and low laser power is a crucial factor in preventing any unwanted particle aggregation or melting.[28] The effect of the initial degree of supersaturation and synthesis pH on the NLA and NLR spectra of ZnTe QDs has also been investigated. In contrast to other techniques, the Z-scan is a quite simple and sensitive one that helps understand the NLO properties of nanocrystals.[29,30] Here, a large third-order NLO susceptibility of 10^{-6} esu is found in ZnTe QDs, even with the low power (15 mW) of the CW He−Ne laser (632.8 nm). Additionally, the figure of merit is also calculated to evaluate the suitability for device applications.

In addition, the ZnTe QDs are isotropically self-assembled into nanoballs, exhibiting profoundly different NLO properties, which are more suitable for optoelectronic device applications. To the best of our knowledge, this is the first such study of NLO properties of differently sized colloidal ZnTe QDs and their self-assembled nanostructures.

2. EXPERIMENTAL SECTION

2.1. Materials. Zinc sulfate (99%), sodium borohydride (99%), telluric acid (98%), propan-2-ol, NaOH, HCl, and thioglycolic acid (98%) were purchased from Sigma-Aldrich and were used without further purification.

2.2. Synthesis and Self-Assembly of ZnTe QDs. ZnTe QDs of different sizes were synthesized by following the supersaturation-controlled method reported by us previously.[23] Throughout the synthesis, a reagent molar ratio was kept constant (Zn^{2+}/TGA/Te^{2-}: 1:2.5:0.5). First, sodium hydrogen telluride (NaHTe) was prepared by the reduction of telluric acid by $NaBH_4$ in the presence of a N_2 atmosphere. Further, the synthesized NaHTe was added to the solution of Zn^{2+} and TGA (Zn^{2+} = 1.6 mM). The degree of supersaturation corresponding to the aforementioned Zn^{2+} and Te^{2-} concentrations was designated as 1S. These syntheses were carried out at pH 6 and 12. By maintaining the constant reagent ratio (Zn^{2+}/TGA/Te^{2-}: 1:2.5:0.5), the concentration of Zn^{2+}-TGA and NaHTe was increased by a factor of 10 for both pH (6 and 12). The degree of supersaturation corresponding to the 10 times increased concentrations of Zn^{2+} and Te^{2-} was designated as 10S.

QDs synthesized at pH 12 were simply stored in the dark for 3 weeks at room temperature, resulting in isotropic self-assembly into nanoballs. All of the synthesis steps and conditions are detailed in Scheme S1 and Table S1.

2.3. Nonlinear Optical Properties. Nonlinear absorption (NLA) and nonlinear refraction (NLR) were measured by the open- and closed-aperture Z-scan technique. The Z-scan technique is one of the most elementary and precise methods to find out the nonlinear parameters.[29,30] In this process, the sample is moved along the Z-direction of a focussed Gaussian beam and the transmittance is measured as a function of the sample position (Z). When the sample is carried toward the focus, the photon flux increases, as a result, positive lensing provides a parallel beam, and this beam broadens at the aperture, which results in a decrease in transmittance. Hence, the sample undergoes a changed incident field, concerning varied Z positions. The optical geometry of the Z-scan is shown in Scheme 1. Here, a continuous-wave (CW) He−Ne laser (TEM00 632.8 nm, 15 mW) with a Gaussian spatial profile is used as a light source. The laser beam is split into nonlinear and reference arms by the beam splitter (BM). Detector D1 is used to detect the input power and its variations, whereas the transmitted intensity is sensed by detector D2.

The beam waist radius was calculated by the knife-edge method and found to be ω_0 = 21.45 μm. The corresponding

https://doi.org/10.1021/acsomega.1c05449
ACS Omega 2021, 6, 31375−31383

Rayleigh length Z_0 ($\pi\omega_0^2/\lambda$) is found to be 2.28 mm; here, λ is the laser wavelength (632.5 nm). Here, the sample thickness or cuvette thickness (L) is 1 mm, which is less than the Rayleigh length ($L \ll Z_0$), and this satisfies the "thin sample" condition.

The third-order absolute nonlinear optical susceptibility ($\chi^{(3)}$) is defined as the addition of a real and imaginary part of the susceptibility.

$$|\chi^{(3)}| = [(\chi_{re}^{(3)})^2 + (\chi_{img}^{(3)})^2]^{1/2} \quad (1)$$

Real part

$$\chi_{re}^{(3)}(\text{esu}) = 10^{-4}\frac{\varepsilon_0 c^2 n_0^2}{\pi} n_2 \left(\frac{\text{cm}^2}{\text{W}}\right) \quad (2)$$

Imaginary part

$$\chi_{img}^{(3)}(\text{esu}) = 10^{-2}\frac{\varepsilon_0 c^2 n_0^2 \lambda}{4\pi^2}\beta \left(\frac{\text{cm}}{\text{W}}\right) \quad (3)$$

where c and ε_0 are the velocity of light and permittivity in vacuum, respectively. The nonlinear absorption coefficient (β) was calculated from the NLA analysis, whereas the nonlinear refractive index (n_2) of the third order was found by the analysis of NLR. In the open aperture, the intensity of the transmitted light ($T(z)$) is measured by the detector, with the translation of the sample or at Z since $T(z)$ depends on linear and nonlinear absorption coefficients, irradiance intensity, the effective length of the sample, and the number of photons (n) absorbed in a single transition. Thus, normalized transmittance for a certain number (n) of photon absorption (nPA) is given by the following equation[29−32]

$$T_{n\text{PA}}(Z) = 1 - \frac{(\alpha_n (I)^{n-1} L_{\text{eff}}^{(n)})}{n^{(3/2)}} \quad (4)$$

In eq 4, $T_{n\text{PA}}$ is the normalized measured transmittance and α_n is the total absorption coefficient for nPA, which is given by eq 5

$$\alpha = \alpha_0 + \beta I \quad (5)$$

where α_0 is the linear absorption coefficient and I is the irradiance of the laser beam within the sample. I or excitation intensity at position z is given by

$$I = \frac{I_0}{1 + (z^2/z_0^2)} \quad (6)$$

where Z_0 is the Rayleigh range and

$$Z_0 = \frac{\pi\omega_0^2}{\lambda} \quad (7)$$

where ω_0^2 is the minimum beam waist at the focal point ($z = 0$) and λ is the laser wavelength. $L_{\text{eff}}^{(n)}$ is calculated by

$$L_{\text{eff}}^{(n)} = [\frac{1 - \exp(-(n-1)\alpha_0 L)}{(n-1)\alpha_0}] \quad (8)$$

where L is the sample length or cuvette width and α_0 is the linear absorption coefficient. The nonlinear refractive index is defined as

$$n_2 = \frac{\Delta\phi_0}{kI_0 L_{\text{eff}}} \quad (9)$$

where ϕ_0 is the nonlinear phase and is given by

$$\left|\Delta\phi_0 = \frac{\Delta T_{pv}}{0.406(1-S)^{0.27}}\right| \quad (10)$$

where ΔT_{pv} is a change in normalized transmittance between the peak and valley and S is a fraction of the beam transmitted by the aperture.

2.4. Other Characterizations. The UV−vis absorption spectra of colloidal ZnTe QDs were taken using a Jasco V-770 spectrophotometer without any dilution. Photoluminescence (PL) measurements were performed at room temperature using a PerkinElmer (LS 55) luminescence spectrometer. The size and shape of QDs were determined by transmission electron microscopy (TEM). High-resolution TEM (HRTEM) images were recorded using a JEM-2010 (JEOL, Japan) at 200 kV operating voltage. The TEM was equipped with a charge-coupled device camera (Gatan, Pleasanton, California). Specimens for TEM were prepared by drop casting the as-prepared QDs on the carbon-coated Cu grids, and the excess solvent was immediately evaporated. X-ray diffraction (XRD) pattern was recorded on a Philips Analytical X-ray B.V. diffractometer type PW 1710 equipped with graphite monochromatic Cu Kα radiation (λ = 1.54 Å).

3. RESULTS AND DISCUSSION

3.1. Synthesis and Characterization. Differently sized water-soluble ZnTe QDs were synthesized by following the supersaturation-controlled method established by us.[23] The synthesis details are shown in Scheme S1 and Table S1. Absorption and photoluminescence spectra of ZnTe QDs synthesized at pH 6 and 12 are shown in Figure 1. The optical absorption and photoluminescence spectra give a very good idea about the monodispersity of semiconductor nanocrystals.

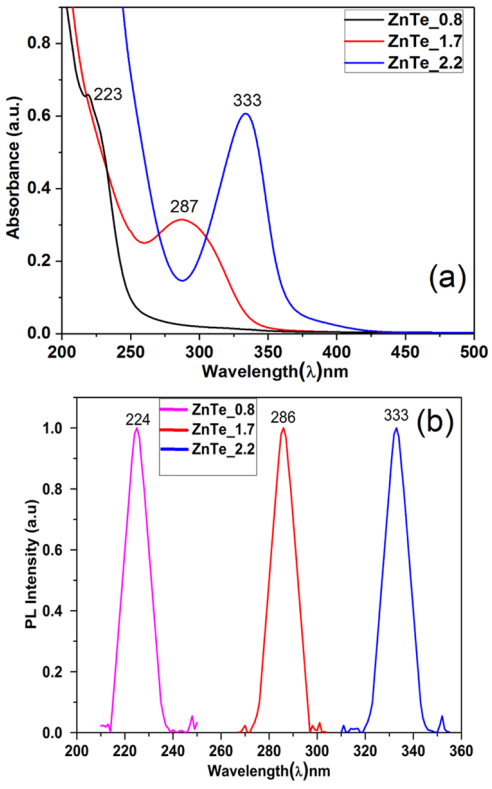

Figure 1. (a) UV−vis absorbance and (b) PL spectra of ZnTe_0.8, ZnTe_1.7, and ZnTe_2.2 QDs.

https://doi.org/10.1021/acsomega.1c05449
ACS Omega 2021, 6, 31375−31383

The as-synthesized ZnTe nanocrystals exhibit tunable band-edge luminescence with an FWHM of 10−12 nm and a symmetric Gaussian profile. As the luminescence is strongly size-dependent in quantum confinement regime, a small value of full-width at half maximum (FWHM) also indicates an extremely narrow size distribution or high monodispersity.

The absorption, as well as the size of QDs, is highly influenced by the degree of supersaturation. The blue shift is attributed to the decrease in the size of QDs.[33−35] At pH 12, the PL peak shifts from 333 to 224 nm for 10 times increment in supersaturation. The degree of supersaturation is the dominant factor responsible for producing smaller sized QDs. When supersaturation increases 10 times (1S → 10S), the size of QDs decreases drastically (63%) from 2.2 to 0.8 nm at pH 12 (Figure 2 and Table S1). Keeping the degree of supersaturation the same (10S), if the pH is changed to 6, 1.7 nm sized QDs are obtained. Thus, by controlling the pH and degree of supersaturation, ZnTe QDs having sizes of 2.2, 1.7, and 0.8 nm were synthesized (hence named ZnTe_2.2, ZnTe_1.7, and ZnTe_0.8, respectively). ZnTe_2.2 QDs further self-assemble into nanoballs, which further self-organize into a necklace-like pattern (ZnTe nanonecklace).

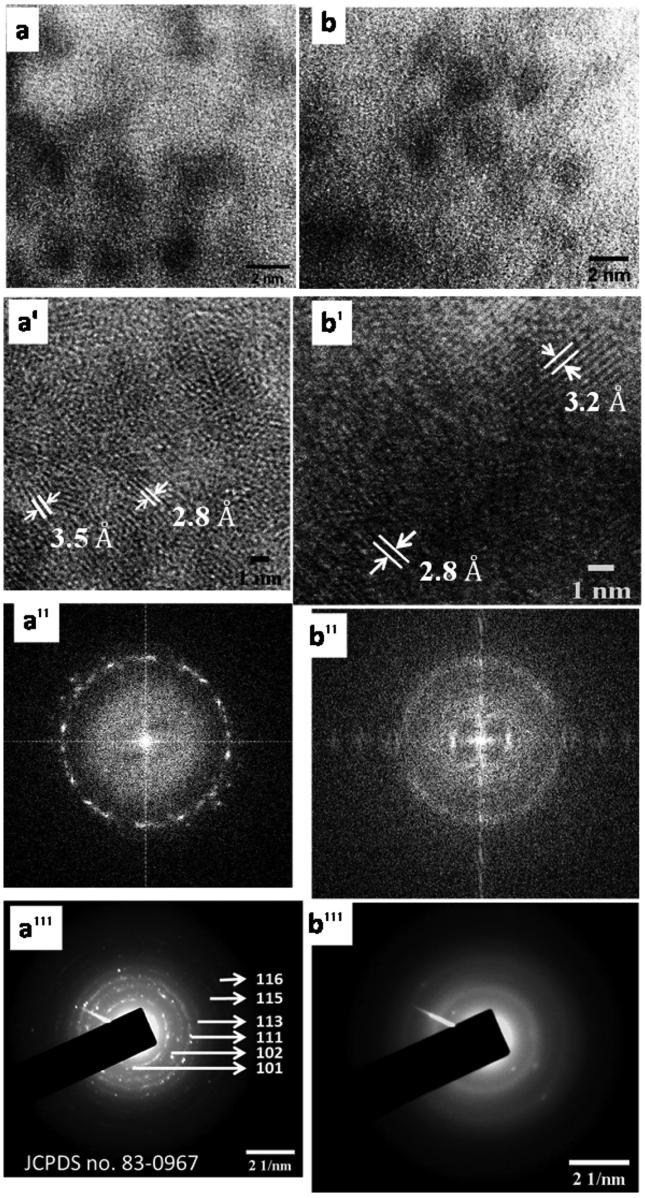

Figure 2. (a, b) Bright-field TEM images, (a′, b′) HRTEM images, (a″, b″) FFT images, and (a‴, b‴) SAED pattern of ZnTe_1.7 and ZnTe_2.2. Size distribution histograms of the corresponding TEM images are shown in Figure S1.

High-resolution TEM (HRTEM) images are shown in Figure 2, and size distribution histograms (Figure S1) are deduced to ascertain the "narrow size distribution" or "high monodispersity" in ZnTe QDs. The standard deviation for ZnTe_2.2 is 0.27 nm, which is reduced to 0.17 nm for ZnTe_1.7. It shows that the size distribution is nearly halved on increasing the relative degree of supersaturation by 10 times.

To further ascertain the crystallinity of the QD samples, FFT patterns were derived from HRTEM images and electron-diffraction experiments were also performed, results of which are shown in Figure 2a″,b″ and a‴,b‴. The SAED pattern of the sample ZnTe_1.7 shows well-resolved six bright rings corresponding to lattice planes having hkl values of 101, 102, 111, 113, 115, and 116 of the hexagonal phase. Bright rings can also be seen in the FFT pattern of the sample. Among the synthesized samples, ZnTe_1.7 possesses the best crystallinity, as evident in FFT and SAED patterns. The hexagonal phase of the nanocrystals was also confirmed by the XRD pattern (Figure S2), and the sizes determined using the peak broadening were in close agreement with the sizes estimated by HRTEM and UV−vis spectroscopy (Table S1).

3.2. Nonlinear Optical Properties. When the as-prepared ZnTe QDs are exposed to intense and coherent light (laser), their polarization shows a nonlinear dependence on the electric field. NLA and NLR of ZnTe QDs of different sizes were investigated using the open- and closed-aperture *Z*-scan technique, respectively. The sample is scanned over 10 mm in both directions and no scattering is observed during the scan. The NLO parameters, two-photon absorption coefficient (β), three-photon absorption coefficient (γ), and nonlinear refractive index (n_2), were calculated by the aforementioned equations (Section 2.3). The NLO data with an open and closed aperture are shown in Figures 3−5. The solvent, deionized water, does not show any NLO response in the same condition (Figure S3). Thus, the observed NLO properties can be attributed solely to the ZnTe QDs. All of the solutions were diluted with deionized water to keep the concentration of ZnTe monomer species constant at 0.2 mM for the *Z*-scan measurements.

3.2.1. Nonlinear Absorption (NLA). The NLA curves were fitted with two-photon absorption (2PA) and three-photon absorption (3PA) models. The NLA curves for ZnTe_0.8 and ZnTe_1.7 are perfectly fitted by the 3PA model while ZnTe_2.2 is perfectly fitted by the 2PA model. As can be seen in Figure S4 and Table S2, the fitting parameter, χ^2 test, for ZnTe_2.2 has a much lower value with the 2PA model. However, for the smaller QDs, ZnTe_1.7 and ZnTe_0.8, the 3PA model shows the best fit with a lower value of χ^2. The finding is in consonance with the electronic band structure diagram shown in Scheme 2. When two photons are absorbed by ZnTe_2.2, it corresponds to an electronic transition from the valence band edge (VBE) to some energy level that lies within the conduction band. However, in ZnTe_0.8 and ZnTe_1.7, if the electrons at the VBE are assumed to absorb two photons of 632.5 nm, they are likely to end up in the forbidden gap region. At least, one additional photon needs to

https://doi.org/10.1021/acsomega.1c05449
ACS Omega 2021, 6, 31375−31383

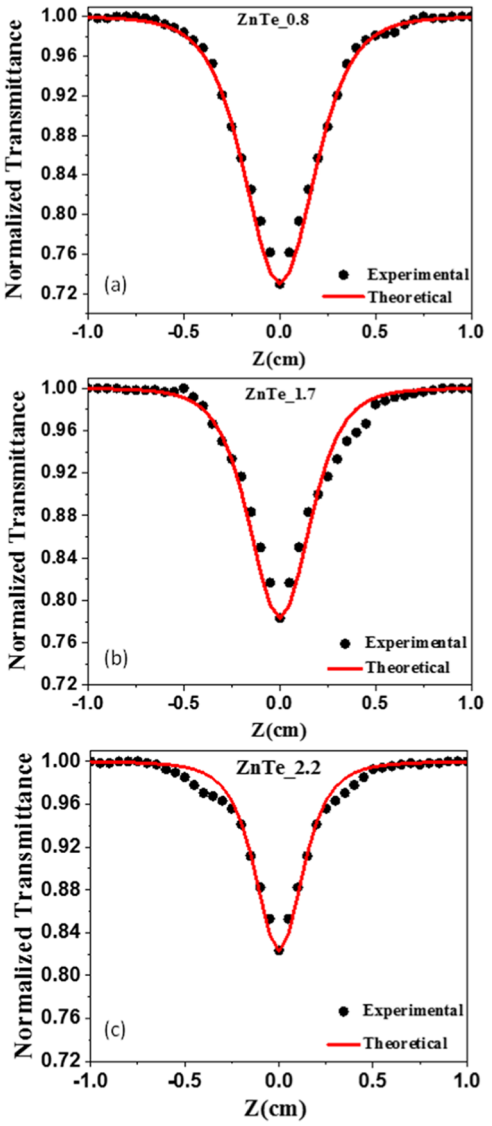

Figure 3. Open-aperture *Z*-scan plots for (a) ZnTe_0.8 and (b) ZnTe_1.7. The experimental data are fitted by the three-photon absorption (3PA) model. [Alternatively, the fitting by the two-photon absorption (2PA) model is shown in Figure S4, and the comparative error analysis of the two models is presented in Table S2.] The open-aperture *Z*-scan plots for (c) ZnTe_2.2. The experimental data are fitted by the two-photon absorption (2PA) model. [Alternatively, the fitting by the two-photon absorption (3PA) model is shown in Figure S4.]

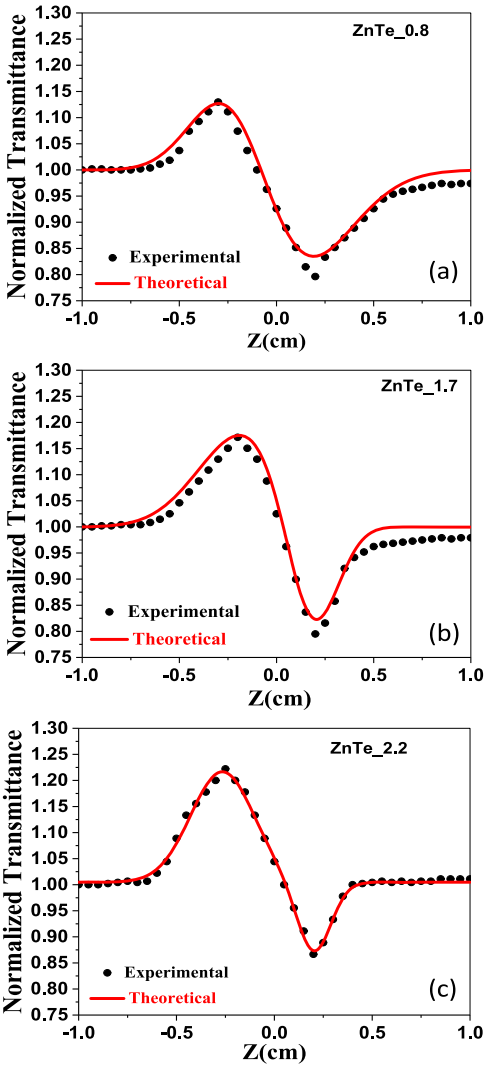

Figure 4. Closed-aperture *Z*-scan plots for (a) ZnTe_0.8, (b) ZnTe_1.7, and (c) ZnTe_2.2.

be absorbed to reach a real energy state in the conduction band region. Thus, the 3PA model vividly explains the NLA behavior in the smaller QDs, ZnTe_0.8 and ZnTe_1.7. Figure S4a–d gives NLA results of ZnTe QDs, with sizes of 0.8, 1.7, and 2.2 nm for the 2PA and 3PA absorption models.

The γ and β values were calculated from the best fitting of NLA curves and found to be 3.00×10^{-4} cm^3/MW^2, 2.21×10^{-4} cm^3/MW^2, and 0.30 cm/MW for ZnTe_0.8, ZnTe_1.7, and ZnTe_2.2, respectively. Further, both in the two- and three-photon models, the NLA coefficient decreases as the diameter of the dots increases.

The role of initial synthesis conditions is also prominently observed. The initial synthesis pH and degree of supersaturation greatly affect the size and crystallinity, which, in turn, affect the NLA properties. The experiments have been performed using a He–Ne CW laser (15 mW; 632.8 nm). The power corresponds to an energy density of approximately 4 kW/cm^2 and it is also sufficient to generate nonlinear effects. Such observations have been reported previously by us[32] as well as by other research groups.[36]

3.2.2. Nonlinear Refraction (NLR). Figure 4 shows the closed-aperture *Z*-scan curves of differently sized QDs. In all samples, a peak appears before the focus and followed by a valley; this implies that the QDs possess self-focusing properties with positive n_2. The calculation of the nonlinear absorption coefficient, NLR coefficient, and overall nonlinear susceptibility is shown in Table S3. As can be seen in Figure 5, β increases drastically ($3.00 \times 10^{-4} \rightarrow 2.21 \times 10^{-4}$ cm/MW) while n_2 decreases gradually ($3.04 \times 10^{-2} \rightarrow 3.6 \times 10^{-2}$ cm^2/MW) as we move from smaller to larger QDs, i.e., ZnTe_0.8 → ZnTe_1.7.

It is important to note here that we have used a low-power laser compared to other researchers.[37] The high-power pulse laser can cause melting and aggregation[38] leading to the structural transformation of crystals, which, in turn, might change the nonlinear optical properties.[39]

In general, both electronic (Kerr effect) and thermal effects could contribute to n_2 in closed-aperture *Z*-scans. In this

https://doi.org/10.1021/acsomega.1c05449
ACS Omega 2021, 6, 31375–31383

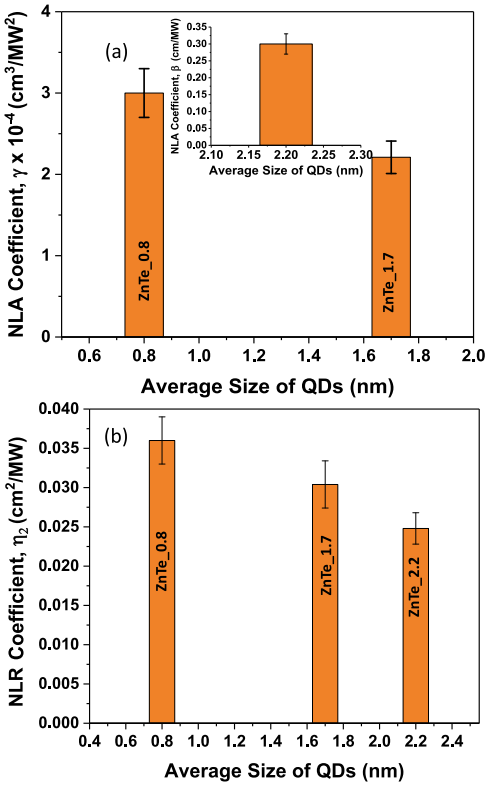

Figure 5. Variation of the (a) NLA and (b) NLR coefficient with the change in average particle size of ZnTe QDs.

Scheme 2. Energy Band Diagram of ZnTe QDs of Different Sizes[a]

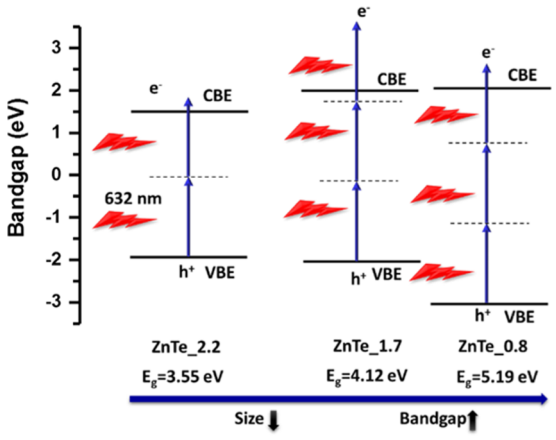

[a] E_g: band gap; CBE: conduction band edge; and VBE: valance band edge.

experiment, the thermal effect is highly suppressed, owing to the very low peak irradiance (I_0 = 4 kW/cm^2). Furthermore, the thermal origin of n_2 is explained by Sheik-Bahae et al.[29] The thermal basis for nonlinearity might be confirmed by the value of ΔZ_{p-v} (the peak−valley separation); if it is of nonthermal origin, then $\Delta Z_{p-v} \approx 1.7z_0$ while for thermal-induced n_2, $\Delta Z_{p-v} \gg 1.7z_0$. In this study, ΔZ_{p-v} is the order of $1.7z_0$ (0.3876 cm) for all of the samples. Values of ΔZ_{p-v} are given in Table S4. Thus, we conclude that the dominating response of the NLR of the ZnTe QDs is the electron Kerr effect.

3.2.3. Optical Nonlinearity in Self-Assembled ZnTe QDs. ZnTe_2.2 QDs possess a unique property to undergo isotropic self-assembly.[23] When ZnTe_2.2 QDs are left to stand in the dark for three weeks at room temperature, a spherical ball-like nanostructure appears, as seen in TEM images. The average diameter of these nanoballs is 100 ± 10 nm. The nanoballs further assemble into pearl necklace-like configurations, ZnTe_NB (Figure 6). As observed in HRTEM image, the average spacing between QDs is less than 1 nm in ZnTe_NB due to which the exciton−exciton coupling[23] occurs, leading to a significant blue shift of 30 nm in the absorption and emission spectra. Furthermore, improved optical nonlinearity is also observed in these hierarchical nanostructures[31] due to the peculiar orientation, organization, and interaction of the QDs. The open-aperture curve of ZnTe_2.2 and ZnTe_NB plotted in Figure 7a shows a symmetric valley with respect to focus (Z = 0). The normalized transmittance at focus gradually increases by the increase in the average diameter of QDs. On fitting the NLA curves, a significant decrease in β by 45% (0.3 → 0.166 cm/MW) was found in comparison to the pristine ZnTe QDs (ZnTe_2.2). ZnTe_NB also follows the 2PA absorption model similar to ZnTe_2.2 as shown in Figure S4 and Table S2. Further, the NLR coefficient, n_2, shows a higher value as compared to ZnTe_2.2, which is an increase by 40% ($2.48 \times 10^{-2} \rightarrow 3.48 \times 10^{-2}$ cm^2/MW), as shown in Figure 8.

Alternatively, the fitting by the three-photon absorption (3PA) model is shown in Figure S4, Supporting Information, and the comparative error analysis of the two models is presented in Table S2.

3.3. Implications for Optoelectronic Devices. For all-optical switching devices with high switching efficiency, a nonlinear optical material is required that has high NLR and low linear and nonlinear absorption. The quality of a nonlinear material is defined in terms of one-photon figure of merit (W), two-photon figure of merit (T), and three-photon figure of merit (V).

$$W = \frac{n_2 I}{\alpha \pi} \tag{11}$$

$$T = \frac{\beta \lambda}{n_2} \tag{12}$$

$$V = \frac{n_2}{\lambda I \gamma} \tag{13}$$

where n_2 is the nonlinear refraction index; α, β, and γ are linear, 2PA, and 3PA absorption coefficients, respectively; and I and λ are the intensity and wavelength of the laser, respectively. A suitable candidate for all-optical switching requires $W > 1$, $T < 1$, and $V < 1$.[38,40,42] The values of W, T, and V are shown in Table S3. ZnTe_0.8 and ZnTe_2.2 are found to be the best QD samples that are suitable for "all-optical" switching device applications.

Further, as the QDs (ZnTe_2.2) self-assemble and transform into nanoballs (ZnTe_NB), the NLR coefficient increases while NLA decreases as shown in Figure 8. The two inherent features complement each other and help perform some of the most complex optical processes.[41] One such application involves making optical waveguides for supercontinuum generation (SCG) spanning visible to the near-infrared (NIR) range. In a previous work by Chu et al.,[43] it has been shown that along with high NLR, the material

https://doi.org/10.1021/acsomega.1c05449
ACS Omega 2021, 6, 31375−31383

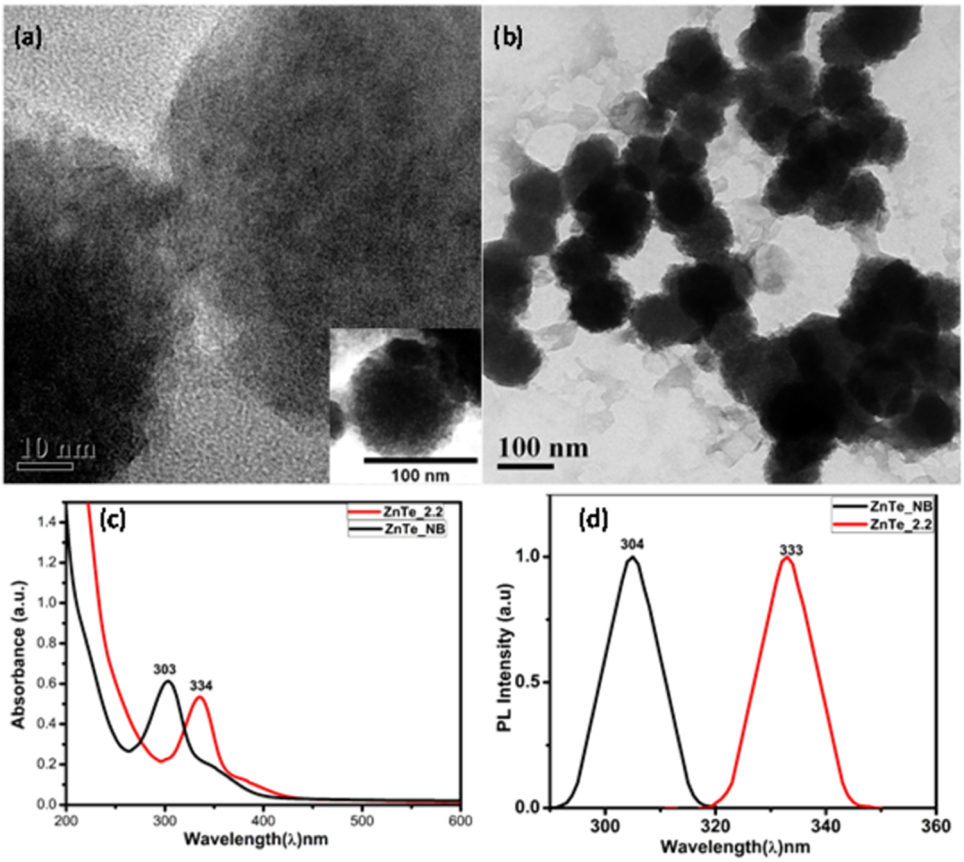

Figure 6. (a) TEM image showing two closely approaching ZnTe nanoballs, inset: a zoomed-in view of a nanoball. (b) TEM image showing self-organization of nanoballs into a pearl necklace type arrangement. (c) Absorption and (d) PL spectra of the ZnTe nanoballs and QDs.

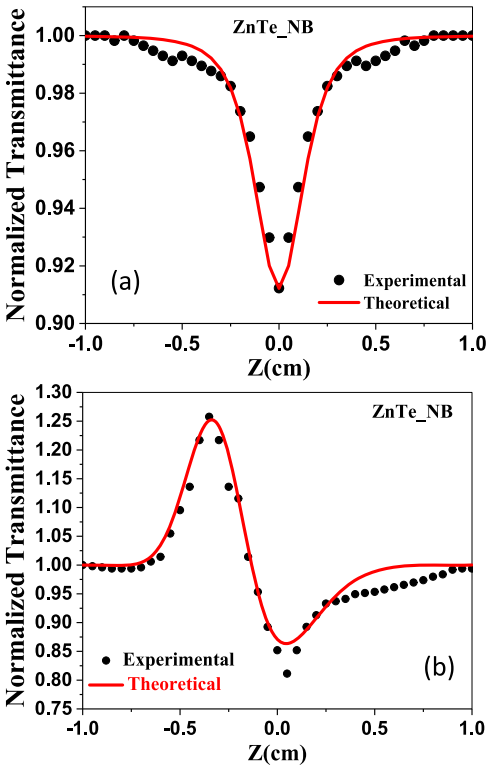

Figure 7. (a) Open-aperture *Z*-scan plot and (b) closed-aperture *Z*-scan plot for ZnTe_NB. The experimental data are fitted by the two-photon absorption (2PA) model.

should also possess a wide band gap. Several high nonlinear materials such as silicon and chalcogenide glasses have low energy band gap, which limits their application. In this context, using ultrasmall ZnTe nanocrystals can be advantageous as quantum confinement leads to the widening of the band gap. Additionally, self-assembly provides another handle to enhance both the NLR and the energy gap. As discussed in the previous section, transformation of QDs into nanoballs brings about a huge blue shift of 30 nm in the absorption spectra (Figure 6c). So, a wide band gap coupled with a high NLR index makes the self-assembled ZnTe nanostructure, a better candidate for superior broadband on-chip supercontinuum generation.

4. CONCLUSIONS

A supersaturation-controlled synthesis of ZnTe QDs has been carried out and their NLO properties have been investigated by the *Z*-scan technique using a low-power He−Ne laser (15 mW, 632.8 nm) in a nonresonant condition. For ZnTe QDs having an average size of 0.8 and 1.7 nm, the three-photon absorption model gives the best fit while the two-photon model was found to fit the nonlinear absorption profiles of ZnTe_2.2 and ZnTe_NB. The nonlinear refractive index (n_2) showed a gradual decrease with the size increasing from 0.8 to 2.2 nm. Our studies further reveal that besides size, the isotropic assembly of quantum dots has a profound influence on the NLR properties. Due to the inter-QD exciton−exciton coupling within the self-assembled nanostructure, ZnTe_NB shows a significant blue shift in absorption and increase in the NLR coefficient. With these insights, the key parameters such as pH and supersaturation can be deftly manipulated to tailor

https://doi.org/10.1021/acsomega.1c05449
ACS Omega 2021, 6, 31375−31383

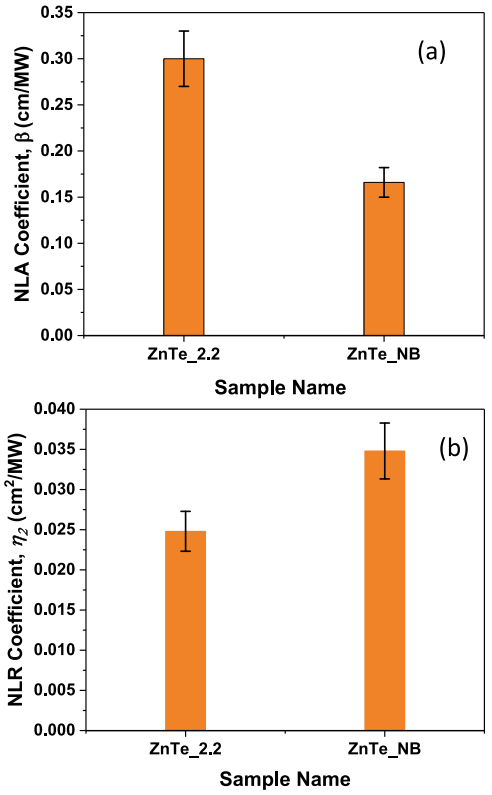

Figure 8. Changes in the (a) NLA and (b) NLR coefficient occur when QD undergoes isotropic self-assembly into nanoballs, having a subnanometer inter-QD separation within the nanoballs.

the NLA, NLR, and the energy gap of ZnTe QDs as required for any intended application. The figure of merit was also evaluated and it was found that ZnTe_0.8 and ZnTe_2.2 QDs are best suited for the fabrication of all-optical switching devices. The self-assembled nanostructures also offer themselves as an attractive alternative to conventional materials in making waveguides for SCG application.

■ ASSOCIATED CONTENT

Supporting Information

The Supporting Information is available free of charge at https://pubs.acs.org/doi/10.1021/acsomega.1c05449.

Synthesis of ZnTe QDs; structural characterization; and nonlinear properties (PDF)

■ AUTHOR INFORMATION

Corresponding Author

Amiya Priyam − *Department of Chemistry, School of Physical and Chemical Sciences, Central University of South Bihar, Gaya 824236, India;* orcid.org/0000-0002-3310-6288; Phone: +91-8521147173; Email: apriyam@cub.ac.in

Authors

Sovan Kumar Patra − *Research and Development Division, Tata Steel Ltd., Jamshedpur 831007, India;* orcid.org/0000-0002-3113-6619

Bhavesh Kumar Dadhich − *Department of Physics, School of Applied Sciences, KIIT, Deemed to be University, Bhubaneswar 751024, India;* Present Address: Department of Physics, Indian Institute of Science Education and Research Mohali, Sahibzada Ajit Singh Nagar, Punjab 140306, India; orcid.org/0000-0003-2670-1713

Bhavya Bhushan − *Department of Physics, School of Applied Sciences, KIIT, Deemed to be University, Bhubaneswar 751024, India;* orcid.org/0000-0001-5073-0640

Ravi Kant Choubey − *Department of Applied Physics, Amity Institute of Applied Sciences (AIAS), Amity University, Noida 201313, India;* orcid.org/0000-0002-3299-9686

Complete contact information is available at: https://pubs.acs.org/10.1021/acsomega.1c05449

Author Contributions

#S.K.P. and B.K.D. contributed equally. The manuscript was written through contributions of all authors. All authors have given approval to the final version of the manuscript.

Notes

The authors declare no competing financial interest.

■ ACKNOWLEDGMENTS

One of the authors (A.P.) gratefully acknowledges the financial support from DST, Govt. of India, under the Nano Mission (ref no. SR/NM/NS-1047/2012) and Fast-Track scheme (ref no. SB/FT/CS-84/2011). A.P. also thanks UGC-DAE CSR, Kolkata Center, for funding under the CRS scheme. One of the authors (B.K.D.) is thankful to CSIR, New Delhi, for the award of the Senior Research Fellowship (SRF). The authors also thank Kumar Indrajit, BIT Mesra, for arranging the experimental setup for NLO measurements.

■ REFERENCES

(1) Tessier, M. D.; Dupont, D.; De Nolf, K.; De Roo, J.; Hens, Z. Economic and Size-Tunable Synthesis of InP/ZnE (E = S, Se) Colloidal Quantum Dots. *Chem. Mater.* **2015**, *27*, 4893−4898.

(2) Martynenko, I. V.; Litvin, A. P.; Purcell-Milton, F.; Baranov, A. V.; Fedorov, A. V.; Gun'Ko, Y. K. Application of Semiconductor Quantum Dots in Bioimaging and Biosensing. *J. Mater. Chem. B* **2017**, *5*, 6701−6727.

(3) Bera, D.; Qian, L.; Tseng, T. K.; Holloway, P. H. Quantum Dots and Their Multimodal Applications: A Review. *Materials* **2010**, *3*, 2260−2345.

(4) Jaliel, G.; Puddy, R. K.; Sánchez, R.; Jordan, A. N.; Sothmann, B.; Farrer, I.; Griffiths, J. P.; Ritchie, D. A.; Smith, C. G. Experimental Realization of a Quantum Dot Energy Harvester. *Phys. Rev. Lett.* **2019**, *123*, No. 117701.

(5) Du, J.; Zhang, M.; Guo, Z.; Chen, J.; Zhu, X.; Hu, G.; Peng, P.; Zheng, Z.; Zhang, H. Phosphorene Quantum Dot Saturable Absorbers for Ultrafast Fiber Lasers. *Sci. Rep.* **2017**, *7*, No. 42357.

(6) Nair, S. V.; Takagahara, T. Theory of Exciton Pair States and Their Nonlinear Optical Properties in Semiconductor Quantum Dots. *Phys. Rev. B* **1997**, *55*, 5153−5170.

(7) Tong, L.; Cheng, J. X. Label-Free Imaging through Nonlinear Optical Signals. *Mater. Today* **2011**, *14*, 264−273.

(8) Dadhich, B. K.; Bhattacharya, S.; Ballav, S.; Bhushan, B.; K Datta, P.; Priyam, A. Femtosecond-Laser-Induced Saturable Absorption and Optical Limiting of Hollow Silver Nanocubes: Implications for Optical Switching and Bioimaging. *ACS Appl. Nano Mater.* **2020**, 11620−11629.

(9) Kiss, N.; Haluszka, D.; Lőrincz, K.; Gyöngyösi, N.; Bozsányi, S.; Bánvölgyi, A.; Szipőcs, R.; Wikonkál, N. Quantitative Analysis on Ex Vivo Nonlinear Microscopy Images of Basal Cell Carcinoma Samples in Comparison to Healthy Skin. *Pathol. Oncol. Res.* **2019**, *25*, 1015−1021.

(10) Hemmer, E.; Benayas, A.; Légaré, F.; Vetrone, F. Exploiting the Biological Windows: Current Perspectives on Fluorescent Bioprobes Emitting above 1000 Nm. *Nanoscale Horiz.* **2016**, *1*, 168−184.

(11) He, G. S.; Yong, K.-T.; Zheng, Q.; Sahoo, Y.; Baev, A.; Ryasnyanskiy, A. I.; Prasad, P. N. Multi-Photon Excitation Properties of CdSe Quantum Dots Solutions and Optical Limiting Behavior in Infrared Range. *Opt. Express* **2007**, *15*, No. 12818.
(12) Valligatla, S.; Haldar, K. K.; Patra, A.; Desai, N. R. Nonlinear Optical Switching and Optical Limiting in Colloidal CdSe Quantum Dots Investigated by Nanosecond Z-Scan Measurement. *Opt. Laser Technol.* **2016**, *84*, 87−93.
(13) Mathew, S.; Saran, A. D.; Joseph, S. A.; Bhardwaj, B. S.; Punj, D.; Radhakrishnan, P.; Nampoori, V. P. N.; Vallabhan, C. P. G.; Bellare, J. R. Nonlinear Optical Characterization and Measurement of Optical Limiting Threshold of CdSe Quantum Dots Prepared by a Microemulsion Technique. *J. Mater. Sci.: Mater. Electron.* **2012**, *23*, 739−745.
(14) Szeremeta, J.; Nyk, M.; Wawrzynczyk, D.; Samoc, M. Wavelength Dependence of Nonlinear Optical Properties of Colloidal CdS Quantum Dots. *Nanoscale* **2013**, *5*, 2388−2393.
(15) Kurian, P. A.; Vijayan, C.; Sathiyamoorthy, K.; Suchand Sandeep, C. S.; Philip, R. Excitonic Transitions and Off-Resonant Optical Limiting in CdS Quantum Dots Stabilized in a Synthetic Glue Matrix. *Nanoscale Res. Lett.* **2007**, *2*, 561−568.
(16) Park, S. H.; Casey, M. P.; Falk, J. Nonlinear Optical Properties of CdSe Quantum Dots. *J. Appl. Phys.* **1993**, *73*, 8041−8045.
(17) Abd El-Sadek, M. S.; Nooralden, A. Y.; Moorthy Babu, S.; Palanisamy, P. K. Influence of Different Stabilizers on the Optical and Nonlinear Optical Properties of CdTe Nanoparticles. *Opt. Commun.* **2011**, *284*, 2900−2904.
(18) Nideep, T. K.; Ramya, M.; V P N, N.; Kailasnath, M. Optical Limiting and Optical Properties of Water Soluble CdTe Quantum Dots Prepared through a Colloidal Chemical Route. *Optik* **2019**, *179*, 1101−1108.
(19) Kumbhakar, P.; Chattopadhyay, M.; Mitra, A. K. Nonlinear Optical Properties of Doped ZnS Quantum Dots. *Int. J. Nanosci.* **2011**, *10*, 177−180.
(20) Kole, A. K.; Gupta, S.; Kumbhakar, P.; Ramamurthy, P. C. Nonlinear Optical Second Harmonic Generation in ZnS Quantum Dots and Observation on Optical Properties of ZnS/PMMA Nanocomposites. *Opt. Commun.* **2014**, *313*, 231−237.
(21) Peng, Y.; Wang, G.; Yuan, C.; He, J.; Ye, S.; Luo, X. Influences of Oxygen Vacancies on the Enhanced Nonlinear Optical Properties of Confined ZnO Quantum Dots. *J. Alloys Compd.* **2018**, *739*, 345−352.
(22) Maikhuri, D.; Purohit, S. P.; Mathur, K. C. Linear and Nonlinear Intraband Optical Properties of ZnO Quantum Dots Embedded in SiO2 Matrix. *AIP Adv.* **2012**, *2*, No. 012160.
(23) Patra, S. K.; Bhushan, B.; Priyam, A. Water-Soluble, Luminescent ZnTe Quantum Dots: Supersaturation-Controlled Synthesis and Self-Assembly into Nanoballs, Nanonecklaces and Nanowires. *Dalton Trans.* **2016**, *45*, 3918−3926.
(24) Zhang, J.; Jin, S.; Fry, H. C.; Peng, S.; Shevchenko, E.; Wiederrecht, G. P.; Rajh, T. Synthesis and Characterization of Wurtzite ZnTe Nanorods with Controllable Aspect Ratios. *J. Am. Chem. Soc.* **2011**, *133*, 15324−15327.
(25) Talapin, D. V.; Lee, J. S.; Kovalenko, M. V.; Shevchenko, E. V. Prospects of Colloidal Nanocrystals for Electronic and Optoelectronic Applications. *Chem. Rev.* **2010**, *110*, 389−458.
(26) Du, X.; Zhang, L.; Dong, G.; Sharafudeen, K.; Wen, J.; Chen, D.; Qian, Q.; Qiu, J. Coloration and Nonlinear Optical Properties of ZnTe Quantum Dots in ZnO-TeO2-P2O5 Glasses. *J. Am. Ceram. Soc.* **2014**, *97*, 185−188.
(27) Tang, Z.; Kotov, N. A.; Giersig, M. Spontaneous Organization of Single CdTe Nanoparticles into Luminescent Nanowires. *Science* **2002**, *297*, 237−240.
(28) Yakovlev, V. V.; Lazarov, V.; Reynolds, J.; Gajdardziska-Josifovska, M. Laser-Induced Phase Transformations in Semiconductor Quantum Dots. *Appl. Phys. Lett.* **2000**, *76*, 2050−2052.
(29) Sheik-Bahae, M.; Said, A. A.; Van Stryland, E. W. High-Sensitivity, Single-Beam N_2 Measurements. *Opt. Lett.* **1989**, *14*, No. 955.
(30) Sheik-Bahae, M.; Said, A. A. L. I. A.; Wei, T. H.; Hagan, D. J.; Van Stryland, E. W. Sensitive Measurement of Optical Nonlinearities Using a Single Beam. *IEEE J. Quantum Electron.* **1990**, *26*, 760−769.
(31) Osborne, D. H., Jr.; Haglund, R. F.; Gonella, F.; Garrido, F. Laser-Induced Sign Reversal of the Nonlinear Refractive Index of Ag Nanoclusters in Soda-Lime Glass. *Appl. Phys. B: Lasers Opt.* **1998**, *66*, 517−521.
(32) Dadhich, B. K.; Kumar, I.; Choubey, R. K.; Bhushan, B.; Priyam, A. Shape and Size Dependent Nonlinear Refraction and Absorption in Citrate-Stabilized, near-IR Plasmonic Silver Nanopyramids. *Photochem. Photobiol. Sci.* **2017**, 1556−1562.
(33) Rogach, A. L. *Semiconductor Nanocrystal Quantum Dots Synthesis, Assembly, Spectroscopy and Applications*; Springer, 2008.
(34) *Handbook of Nanophysics: Nanoparticles and Quantum Dots*, 1st ed.; Sattler, K. D., Ed.; CRC Press, 2016.
(35) Sapra, S.; Sarma, D. D. Evolution of the Electronic Structure with Size in II-VI Semiconductor Nanocrystals. *Phys. Rev. B* **2004**, *69*, No. 125304.
(36) Moslemi, Z.; Soheyli, E.; Ara, M. M.; Sahraei, R. Facile preparation of yellow and red emitting ZnCdSeS quantum dots and their third-order nonlinear optical properties. *J. Phys. Chem. Solids* **2018**, *120*, 64−70.
(37) Wu, W.; Ren, S.; Han, Q.; Gao, Y.; Kong, D. Ultrafast Spectroscopic Studies of Composition-Dependent near-Infrared-Emitting Alloyed CdSeTe Quantum Dots. *Phys. Chem. Chem. Phys.* **2018**, *20*, 23556−23563.
(38) Link, S.; Wang, Z. L.; El-Sayed, M. A. How Does a Gold Nanorod Melt? *J. Phys. Chem. B* **2000**, *104*, 7867−7870.
(39) Olszak, P. D.; Webster, S.; Padilha, L. A.; Cirloganu, C. M.; Woodall, M.; Hagan, D. J.; Van Stryland, E. W. In *Energy Bandgap Dependence of Three-Photon Absorption in Semiconductors*, Nonlinear Optics: Materials, Fundamentals and Applications; Optical Society of America, 2007; p WC5.
(40) Shi, W.; Chen, Z.; Liu, N.; Lu, H.; Zhou, Y.; Cui, D.; Yang, G. Nonlinear Optical Properties of Self-Organized Complex Oxide Ce:BaTiO3 Quantum Dots Grown by Pulsed Laser Deposition. *Appl. Phys. Lett.* **1999**, *75*, 1547−1549.
(41) Tocci, M. D.; Bloemer, M. J.; Scalora, M.; Dowling, J. P.; Bowden, C. M. Thin-Film Nonlinear Optical Diode. *Appl. Phys. Lett.* **1995**, *66*, 2324−2326.
(42) He, J.; Qu, Y.; Li, H.; Mi, J.; Ji, W. Three-photon absorption in ZnO and ZnS crystals. *Opt. Express* **2005**, *13*, 9235−9247.
(43) Chu, A.-K.; Lee, C.-K.; Liu, C.-W.; Liu, C.-Y.; Wu, C.-L.; Qiao, J.; Shih, M.-H.; Hwang, P.-S.; Fan, R.; Chiu, Y.-J.; Chu, A. K.; et al. Visible to Near-Infrared Octave Spanning Supercontinuum Generation in Tantalum Pentoxide (Ta_2O_5) Air-Cladding Waveguide. *Opt. Lett.* **2019**, *44*, 1512−1515.

https://doi.org/10.1021/acsomega.1c05449
ACS Omega 2021, 6, 31375−31383